JACS Au
AN OPEN ACCESS JOURNAL OF THE AMERICAN CHEMICAL SOCIETY

pubs.acs.org/jacsau
Article

Low-Temperature Oxidation of Methane on Rutile TiO_2(110): Identifying the Role of Surface Oxygen Species

Yuemiao Lai,[#] Ruimin Wang,[#] Yi Zeng, Fangliang Li,* Xiao Chen, Tao Wang, Hongjun Fan,* and Qing Guo*

Cite This: *JACS Au* 2024, 4, 1396−1404

Read Online

ACCESS | Metrics & More | Article Recommendations | Supporting Information

ABSTRACT: Understanding the microkinetic mechanism underlying photocatalytic oxidative methane (CH_4) conversion is of significant importance for the successful design of efficient catalysts. Herein, CH_4 photooxidation has been systematically investigated on oxidized rutile(R)-TiO_2(110) at 60 K. Under 355 nm irradiation, the C−H bond activation of CH_4 is accomplished by the hole-trapped dangling O_{Ti}^- center rather than the hole-trapped O_b^- center via the Eley−Rideal reaction pathway, producing movable $CH_3^\bullet$ radicals. Subsequently, movable $CH_3^\bullet$ radicals encounter an O/OH species to form CH_3O/CH_3OH species, which could further dissociate into CH_2O under irradiation. However, the majority of the $CH_3^\bullet$ radical intermediate is ejected into a vacuum, which may induce radical-mediated reactions under ambient conditions. The result not only advances our knowledge about inert C−H bond activation but also provides a deep insight into the mechanism of photocatalytic CH_4 conversion, which will be helpful for the successful design of efficient catalysts.

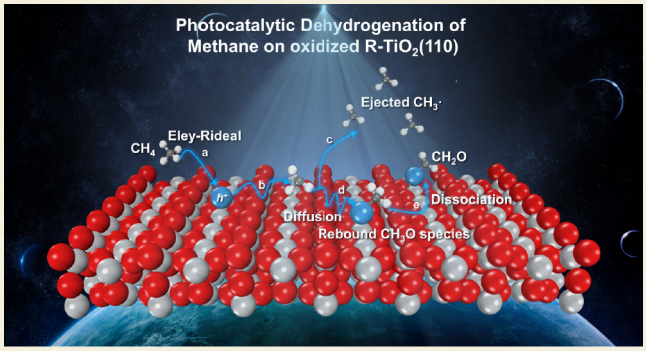

KEYWORDS: *oxidative dehydrogenation of methane, TiO_2 photocatalysis, $CH_3^\bullet$ radical, dangling O_{Ti} atoms, Eley−Rideal mechanism*

INTRODUCTION

With the vigorous exploitation of shale gas and fired ice in recent years, methane (CH_4), as a promising alternative to other fossil fuels, becomes a main source of energy and chemical feedstock in the future.[1−4] Compared with exothermic combustion, direct and selective conversion of CH_4 to high-value-added chemicals is a win-win strategy for maximizing the value of CH_4 while reducing carbon emissions in the atmosphere.[2,4−9] In industry, the conversion of CH_4 into valuable chemicals occurs via an indirect route, in which CH_4 is converted to syngas via the steam reforming process (SRM) first, and is then followed by further synthesizing liquid hydrocarbons via the Fischer−Tropsch (FT) process.[2,4,5,9,10] However, the high C−H bond energy (434 kJ·mol^{-1}), nonpolar derived from high symmetry, and negligible electron affinity of CH_4 make the selective C−H bond activation and conversion of CH_4 via thermocatalysis very challenging and be regarded as the 'holy grail' in catalysis.[2,5,7,9−12]

Alternatively, photocatalysis is a promising approach that can exploit clean solar energy to overcome the barrier of chemical reactions under ambient conditions, resulting in the conversion of CH_4 into value-added oxygenate products smoothly.[3,7,12−15] Generally, photocatalytic oxidation of CH_4 can be classified into catalytic activation and noncatalytic activation.[5] The mechanism of noncatalytic activation has been elaborated that the initial C−H bond activation of CH_4 is induced by photogenerated $^\bullet$OOH or hydroxyl ($^\bullet$OH) radicals following the hydrogen atom transfer (HAT) process, forming possible methyl radicals ($CH_3^\bullet$) intermediate, which are further converted into oxygenates.[3,5,16,17] In contrast, in catalytic activation, both experimental and theoretical studies propose that lattice O^- centers formed by trapping photogenerated holes are the active species for the $CH_3^\bullet$ radical formation from CH_4 over ZnO, TiO_2, and MgO catalysts.[2,7,8,18−21]

However, although the $CH_3^\bullet$ radical is proposed to be the primary intermediate from the initial C−H bond activation of CH_4 under irradiation, due to the low concentration of the $CH_3^\bullet$ radical intermediate and the limitations of detection methods, the evidence of the $CH_3^\bullet$ radical intermediate formation in most reactions is still lacking, which makes the proposed reaction mechanism not indisputable. Therefore, a detailed investigation of the microkinetic mechanism under-

Received: December 6, 2023
Revised: March 6, 2024
Accepted: March 7, 2024
Published: March 26, 2024

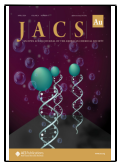

https://doi.org/10.1021/jacsau.3c00771
JACS Au 2024, 4, 1396−1404

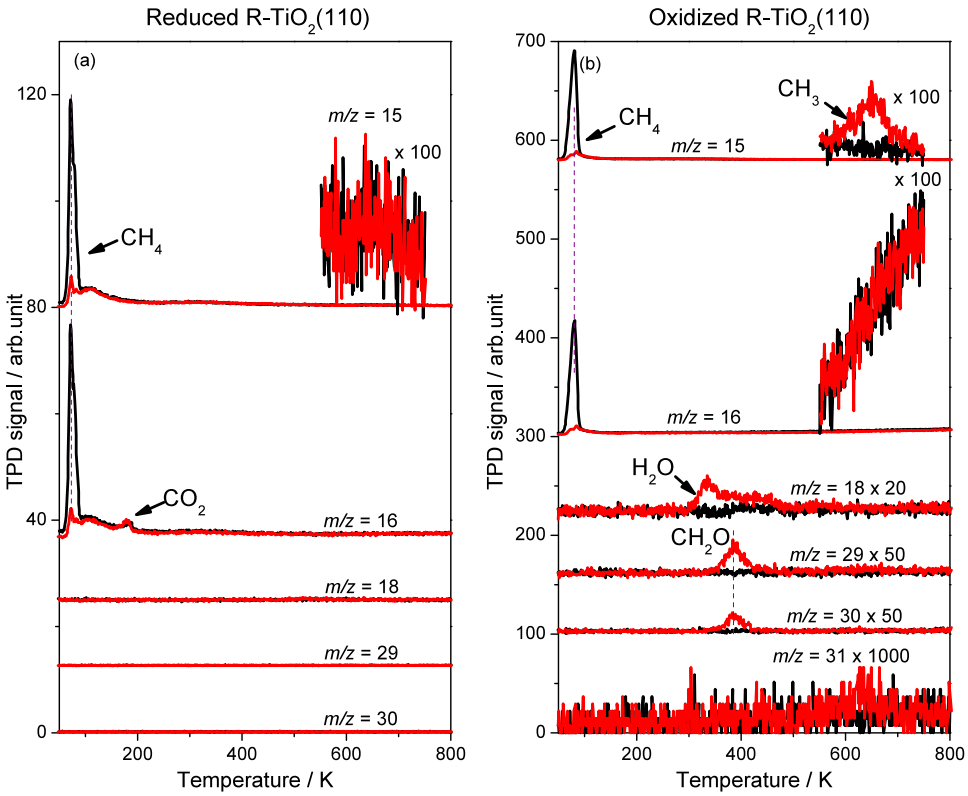

Figure 1. Typical TPD spectra acquired at m/z = 15 (CH_3^+), 16 (CH_4^+ and O^+), 18 (H_2O^+), 29 (CHO^+), 30 (CH_2O^+) and 31 (CH_3O^+) after irradiating the 0.2 L CH_4-covered (a) reduced and (b) oxidized R-TiO_2(110) surfaces for 0 min (black lines) and 10 min (red lines) with 355 nm at 60 K, respectively. The oxidized R-TiO_2(110) surfaces were prepared by exposing reduced surfaces to 200 L O_2 at 300 K. The photon flux of 355 nm light is 2.0×10^{16} photons cm^{-2} s^{-1}.

lying photocatalytic CH_4 conversion with a TiO_2 model catalyst could not only advance our knowledge on photocatalytic C−H bond activation and CH_4 conversion but also be helpful for the development of improved catalysts.

Herein, we report the investigation of the C−H bond activation of CH_4 on oxidized rutile(R)-TiO_2(110), using temperature-programmed desorption (TPD), photo-stimulated desorption (PSD), and density functional theory (DFT) methods. Photooxidation of CH_4 has been achieved on oxidized R-TiO_2(110) at 60 K. The sensitive detection of the $CH_3^\bullet$ radical intermediate demonstrates that the C−H bond activation of CH_4 into the $CH_3^\bullet$ radical is the initial step for CH_4 photooxidation. In combination with the DFT result, the mechanism of CH_4 photooxidation on TiO_2 has been illustrated unambiguously for the first time, in which the hole-trapped dangling O atoms on the Ti_{5c} sites (O_{Ti}^-) are significant active sites.

RESULTS

TPD Results of CH_4 Oxidation

Figure 1 shows the typical TPD spectra of mass-to-charge ratios (m/z) of 15 (CH_3^+), 16 (CH_4^+ and O^+), 18 (H_2O^+), 29 (CHO^+), 30 (CH_2O^+), and 31 (CH_3O^+) collected on the reduced and oxidized R-TiO_2(110) surfaces after adsorbing 0.2 Langmuir (L) CH_4 on the surfaces, followed by 355 nm irradiation for 0 (black line) and 10 min (red line). The oxidized surfaces were prepared by exposing the reduced R-TiO_2(110) surfaces to 200 L O_2 at 300 K, resulting in the major adsorption of O_{Ti} atoms of R-TiO_2(110) and healing the bridging oxygen vacancy sites (O_v).[22,23] Before irradiation, one desorption peak at 70 K appears in the TPD traces of m/z = 15 and 16 on both reduced and oxidized surfaces, which is attributed to the desorption of CH_4 on the Ti_{5c} sites ($CH_{4(Ti)}$).[24] While a broad tail from 90 to 190 K is also observed, which is likely due to the desorption of CH_4 from the sample holder.[24] In addition, a peak at ∼190 K in the TPD trace of m/z = 16 is also observed, which is due to the fragmentation of adsorbed CO_2 from the background (see details in Figure S1). No observation of any product signal illustrates that no thermochemistry of CH_4 occurs during the TPD process on both reduced and oxidized R-TiO_2(110).

After 355 nm irradiation, the $CH_{4(Ti)}$ peak decreases significantly on a reduced R-TiO_2(110). However, no signals of products are detected in the TPD traces, indicating that the decay of CH_4 on the surface is due to photo-induced desorption, and the O_b atom of R-TiO_2(110) is inactive for CH_4 oxidation under current conditions. In contrast, three new desorption features at 330 K (m/z = 18), 385 K (m/z = 29 and 30), and 650 K (m/z = 15) appear on the CH_4-covered oxidized R-TiO_2(110) surface (Figure 1b) after irradiation. The peak at 330 K (m/z = 18) with a broad tail (360−490 K) can be only assigned to the H_2O formation, which is attributed to the desorption of H_2O molecules on the Ti_{5c} sites (H_2O_{Ti}) and the recombinative desorption of terminal OH groups on the Ti_{5c} sites (OH_{Ti}), respectively.[25] Concomitant to the H_2O formation, the CH_2O product (the 385 K peak) is detected in the TPD traces of m/z = 29 and 30, which is due to the desorption of CH_2O molecules on the Ti_{5c} sites (CH_2O_{Ti}) (Figures S2,S3),[26,27] demonstrating that CH_4 conversion via photooxidation occurs on the oxidized R-TiO_2(110) surface.

https://doi.org/10.1021/jacsau.3c00771
JACS Au 2024, 4, 1396−1404

In addition, the small peak at 650 K (m/z = 15) is also detected at the TPD traces of higher masses (including m/z = 16, 29, 30, 31), indicating that the peak is contributed by the desorption of CH_3 groups on the bridging oxygen rows (O_b, CH_3O_b) (See details in Figure S4). However, this peak does not appear in the TPD traces of m/z = 15 on the CH_4-covered reduced R-TiO_2(110) surface (Figure 1a), suggesting that the formation of CH_3O_b is unlikely due to CH_4 activation by O_b under 355 nm irradiation. Otherwise, the peak should be detected on the reduced surface as well. Moreover, the formation of CH_2O_{Ti}, H_2O_{Ti}, and OH_{Ti} products illustrates that the O_{Ti} atom is the exclusively active species in CH_4 photooxidation on R-TiO_2(110).

To further unravel the mechanism of photooxidative CH_4 conversion on R-TiO_2(110), the formation of CH_2O_{Ti}, CH_3O_b, and H_2O_{Ti} products were monitored by the TPD traces of m/z = 15, 18, and 29 from the 0.2 L CH_4-covered oxidized R-TiO_2(110) surfaces as a function of irradiation time (Figure 2a−c). And the yields of CH_2O_{Ti} and H_2O_{Ti} as a function of irradiation time are plotted in Figure 2d. Due to the weak adsorption of CH_4 on R-TiO_2(110), the quantification of the coverage of CH_4 is very difficult, only the normalized integrated area is used to represent the change in the amount of CH_4 (Figure 2d). With an increasing irradiation time, the $CH_{4(Ti)}$ peak at 70 K (m/z = 15) is gradually depleted. Concomitant with the decrease of the $CH_{4(Ti)}$ peak, both the intensities of CH_2O_{Ti} (m/z = 29) and H_2O_{Ti} (m/z = 18) products increase obviously and then reach saturation at long-time irradiation. However, the yield of H_2O_{Ti} formation is always bigger than that of CH_2O_{Ti} (Figure 2d). At 600 s irradiation, the yields of CH_2O_{Ti} and H_2O_{Ti} products reach 0.006 and 0.026 ML, respectively. Once one CH_2O_{Ti} molecule is formed via CH_4 photooxidation, two H atoms will be left on the surface, resulting in the formation of one H_2O_{Ti} molecule.

$$CH_{4(Ti)} + 2O_{Ti} + h^+ \rightarrow CH_2O_{Ti} + H_2O_{Ti} \quad (1)$$

The much higher yield of H_2O_{Ti} indicates that other reaction channels of CH_4 oxidation exist. One channel is the formation of CH_3O_b (m/z = 15 in Figure 2a).

However, the formation of CH_3O_b is rapidly saturated after irradiating the surface for 0.5 s, demonstrating that CH_3O_b formation is not the main channel for CH_4 conversion.

PSD and TOF Evidence of $CH_3^{\bullet}$ Radical Formation

To figure out the possible reaction channels for the large amount of H_2O formation on R-TiO_2(110), the photo-simulated desorption (PSD) spectra were acquired at m/z = 14 (CH_2^+), 15 (CH_3^+), 16 (CH_4^+ and O^+), and 32 (O_2^+) from the 0.2 L CH_4-covered reduced (black lines) and oxidized (red lines) R-TiO_2(110) surfaces during the 355 nm irradiation, respectively (Figure 3). On the reduced surface, no PSD signal of O_2 is detected at m/z = 32. While a very slow increase of the PSD signals at m/z = 14, 15, and 16 is detected when the light is on, which is attributed to the CH_4 desorption (Figure S1). Such a broad desorption is totally different from that of hole-induced O_2 photodesorption on R-TiO_2(110).[28] Therefore, the CH_4 desorption may be due to a thermal desorption process, in which the slow increase of surface temperature under 355 nm irradiation results in the slow desorption of CH_4. Conversely, a sharp increase of the PSD signals at all masses is detected on the oxidized surface immediately when the light is on, similar to previous work about O_2 photo-desorption on R-TiO_2(110).[28] The PSD signal observed at m/z = 32 is due to the desorption of O_2, which is from the adsorption of residual O_2 produced during the oxidized surface preparation procedure. The fragment of O_2 will also contribute to the PSD signal at m/z = 16. As shown in Figure S5, the ratio of the relative intensities of the O_2 fragments at m/z = 16 and 32 is 0.33:1. After subtraction of the contribution of O_2 in the PSD signal at m/z = 16, the shape of the remaining PSD signal (Figure 3g) is very similar to that on the reduced surface, indicating that the thermal CH_4 desorption occurs on both the reduced and oxidized R-TiO_2(110) surfaces. And as shown in

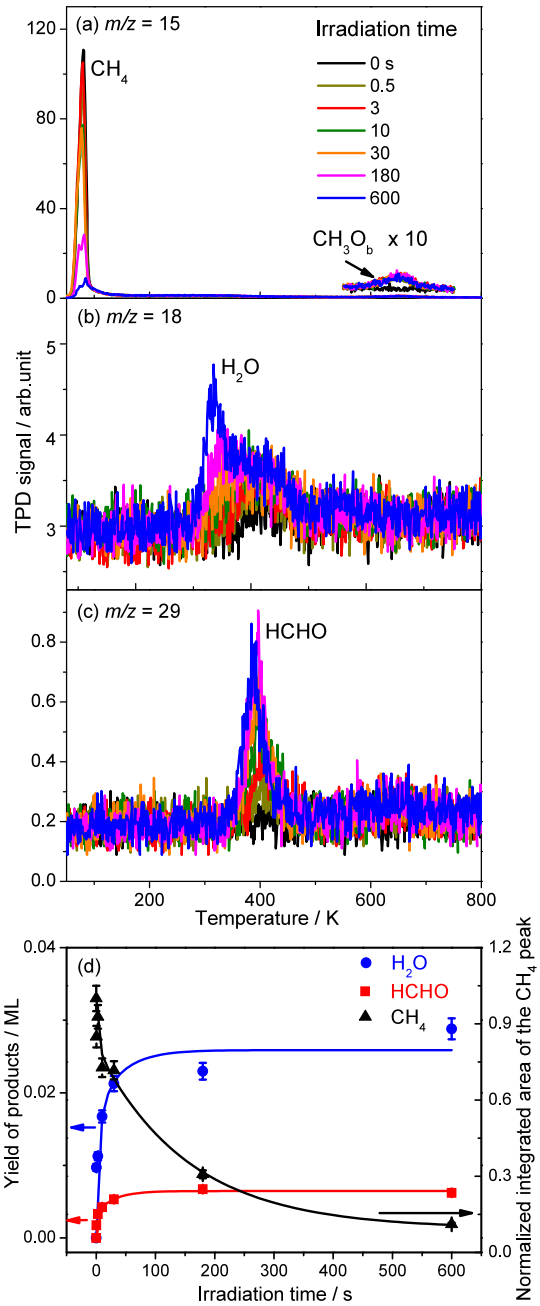

Figure 2. Typical TPD spectra acquired at (a) m/z = 15 (CH_3^+), (b) 18 (H_2O^+), and (c) 29 (CHO^+) on the 0.2 L CH_4-covered oxidized R-TiO_2(110) surfaces as a function of irradiation time, respectively. (d) The yields of H_2O (blue circle), CH_2O (red square), and the normalized integrated area (black triangle) as a function of irradiation time, obtained from a−c. All the plotted lines are only to guide the eye.

https://doi.org/10.1021/jacsau.3c00771
JACS Au 2024, 4, 1396−1404

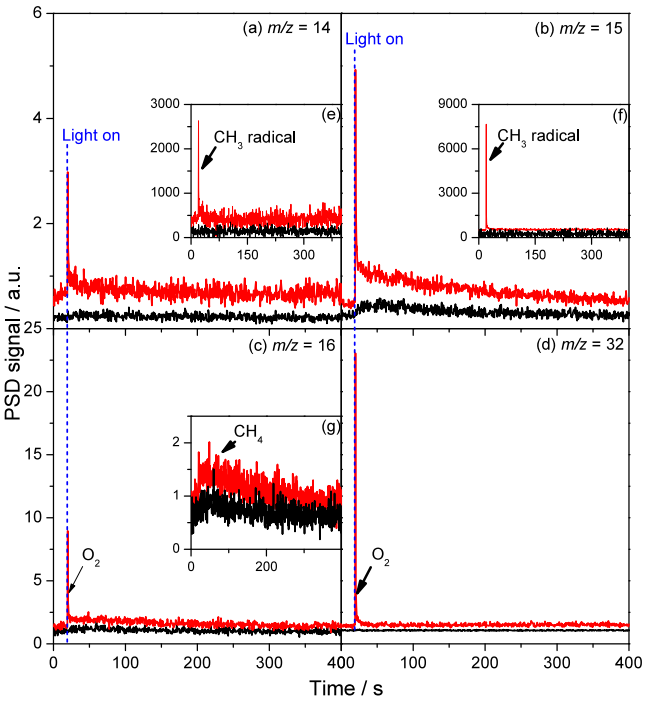

Figure 3. Typical PSD spectra acquired at (a) m/z = 14 (CH_2^+), (b) 15 (CH_3^+), (c) 16 (CH_4^+ and O^+), and (d) 32 (O_2^+) on the 0.2 L CH_4-covered reduced (black lines) and oxidized (red lines) R-TiO_2(110) surfaces during 355 nm irradiation, respectively. e,f) The PSD spectra of m/z = 14 (CH_2^+) and 15 (CH_3^+) in a and b after subtracting the contribution from thermal CH_4 desorption. g) The PSD spectra of m/z = 16 (CH_4^+) in c after subtracting the contribution of photo-induced O_2 desorption (d). The time when the laser is turned on has been marked with blue dotted lines in all of the figures.

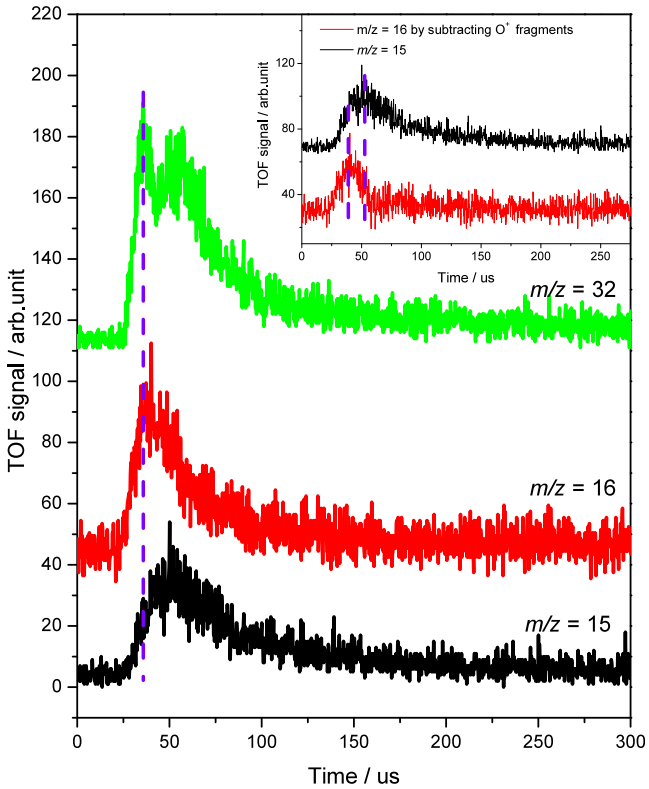

Figure 4. TOF signals collected at m/z = 15 (CH_3^+), 16 (CH_4^+ and O^+), and 32 (O_2^+) as a function of the flight time when the 0.2 L CH_4-covered oxidized R-TiO_2(110) surfaces is irradiated with 343 nm. The inset shows the TOF signals of m/z = 16 (CH_4^+) after subtracting the fragment of O^+ and m/z = 15 (CH_3^+). The photon flux of 343 nm light is 2.0×10^{16} photons cm^{-2} s^{-1}.

Figure S1, the ratio of the relative intensities of CH_4 fragmentations at m/z = 14, 15, and 16 is 0.26:0.96:1. Therefore, after subtracting the contribution of thermal CH_4 desorption in the PSD signals of m/z = 14 and 15, Figure 3e,f are obtained. The sharp peaks should be assigned to the $CH_3^\bullet$ radical rather than molecular CH_4 desorption, based on previous studies.[2,7,8,18,19]

In order to further monitor the individual signal of the ejected $CH_3^\bullet$ radical, typical time-of-flight (TOF) spectra were collected at m/z = 15 (CH_3^+), 16 (CH_4^+ and O^+), and 32 (O_2^+) on the 0.2 L CH_4-covered oxidized R-TiO_2(110) surfaces, as shown in Figure 4. Similar to the PSD results, the TOF signal of m/z = 32 is due to the desorption of the O_2. Due to the better time resolution, two peaks of O_2 desorption can be observed, which are assigned to physically adsorbed and chemically adsorbed O_2 on R-TiO_2(110), respectively.[28] Similarly, the fragment of O_2 will also contribute to the TOF signal at m/z = 16 (O^+). After subtracting the contribution of O^+, the TOF signals of m/z = 16 (CH_4^+) and 15 (CH_3^+) are shown in the inset. The peak of m/z = 16 appears at ~40 μs, which is due to CH_4 desorption. In contrast, the peak of m/z = 15 appears at ~50 μs, suggesting that the peak is contributed by a certain product. As discussed above, it should be due to the ejected $CH_3^\bullet$ radical. Further, the big difference between the yields of H_2O_{Ti} and CH_2O_{Ti} (Figure 2d) demonstrates that the $CH_3^\bullet$ radical is the main product from photooxidative CH_4 conversion on oxidized R-TiO_2(110).

According to previous works,[2,3,6,7,12−17,19,29−31] $CH_3^\bullet$ radical is proposed to be the critical intermediate for photooxidative CH_4 conversion. However, the step of $CH_3^\bullet$ radical formation is always ambiguous because of the absence of direct evidence for the $CH_3^\bullet$ radical intermediate formation. Here, the observation of $CH_3^\bullet$ radical, H_2O_{Ti} and CH_2O_{Ti} products on the oxidized R-TiO_2(110) surface under 355 nm irradiation illustrates that $CH_3^\bullet$ radical is produced via the reaction between CH_4 and active O_{Ti} rather than O_b. Based on previous work about photocatalytic propane (C_3H_8) conversion on R-TiO_2(110),[32] the active O_{Ti} species is hole-trapped O_{Ti}^- center, which can directly abstract a H atom from the C_3H_8 molecule. Likewise, once $CH_3^\bullet$ radical is formed via a similar process, leaving behind OH species on the Ti_{5c} sites (OH_{Ti}) on the surface, it can diffuse on the surface or eject into the vacuum due to its weak interaction with the surface.[4,8] Subsequently, a small amount of $CH_3^\bullet$ radicals could encounter O_{Ti}, OH_{Ti}, or O_b to form CH_3O_{Ti}, CH_3OH_{Ti}, and CH_3O_b species via the radical-rebound mechanism.[19,33−36] Correspondingly, the CH_3O_b species is observed (650 K peak in the TPD trace of m/z = 15, Figure 1b). Due to the photoreactivity of CH_3OH_{Ti} and CH_3O_{Ti} groups,[37] they can dissociate into CH_2O_{Ti} easily under 355 nm irradiation, leading to no obvious signal of CH_3OH_{Ti} and CH_3O_{Ti} on the surface.

Energy Profiles of CH_4 Conversion by DFT Calculations

To provide a more detailed mechanistic model for photo-oxidative CH_4 conversion on R-TiO_2(110), theoretical

https://doi.org/10.1021/jacsau.3c00771
JACS Au 2024, 4, 1396−1404

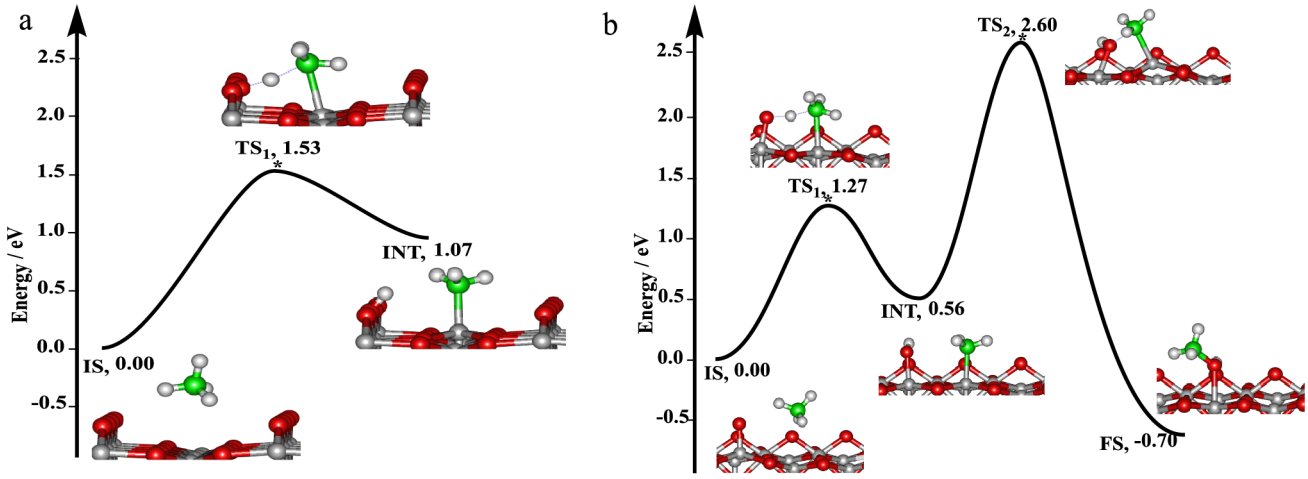

Figure 5. Energy profiles of thermocatalytic CH_4 oxidation on the (a) stoichiometric and (b) oxidized R-TiO_2(110) surfaces. The Ti, O, C, and H atoms are represented as gray, red, green, and white spheres, respectively.

calculations about the adsorption of CH_4, oxidative CH_4 conversion via thermal process, and photoprocess on the R-TiO_2(110) surface were performed (theoretical details are depicted in SI), respectively. As shown in Figure 5a,b, the energy profiles of the initial C−H bond activation of CH_4 via the thermal process on both the stoichiometric and oxidized R-TiO_2(110) surfaces are described, respectively. For the case of thermal C−H bond activation of CH_4, the cleavage of the C−H bond is endothermic by 1.07 eV with a barrier of 1.53 eV on the stoichiometric R-TiO_2(110) surface (Figure 5a). By comparison, on the oxidized R-TiO_2(110) surface, the cleavage of the C−H bond is endothermic by 0.56 eV with a barrier of 1.27 eV (Figure 5b). Then the CH_3 and OH moieties adsorbed on the surface (*CH_3 and *OH) combine to produce CH_3OH, and this step is exothermic by 1.26 eV with an energy barrier of 2.04 eV. The absorption energies (E_{ads}) of CH_4 on both the stoichiometric and oxidized R-TiO_2(110) surfaces are merely ∼0.30 eV, which is much lower than that of C_3H_8 (0.60 eV).[32] Because of the high energy barrier, endothermic nature, and low absorption energy, the initial C−H bond activation via thermal processes on both the stoichiometric and oxidized R-TiO_2(110) surfaces is thermodynamically infeasible, which is in agreement with our TPD results (Figure 1).

By introducing a hole into the oxidized R-TiO_2(110) surface, the hole will be trapped at the O_{Ti} sites preferentially instead of the O_b sites,[32,38] and the energy profile of CH_4 oxidation changes dramatically (Figure 6). According to a recent result about photooxidative dehydrogenation of C_3H_8 on R-TiO_2(110),[32] after an O_{Ti} trapping a hole to form an O_{Ti}^- center, the hole will spontaneously transfer between the O_{Ti} and C_3H_8 molecules, and finally induce C−H bond cleavage. For the case of CH_4 photooxidation, the hole is also trapped by an O_{Ti} atom, forming the O_{Ti}^- center initially (Initial State, IS). Subsequently, the hole will be separated by the CH_4 and the O_{Ti}^- centers and located between each other (Transient State 1, TS_1). Then, the hole will totally transfer to the C atom of CH_4 to form a $CH_3^\bullet$ radical accompanied by C−H bond cleavage, and the dissociated H atom transfers to the adjacent O_{Ti} atom, forming an OH_{Ti} group (*OH). In the whole process, the initial C−H bond activation of CH_4 to *CH_3 is exothermic by 0.64 eV with a barrier of 0.10 eV. Then, the *CH_3 and *OH can combine to produce CH_3OH via the

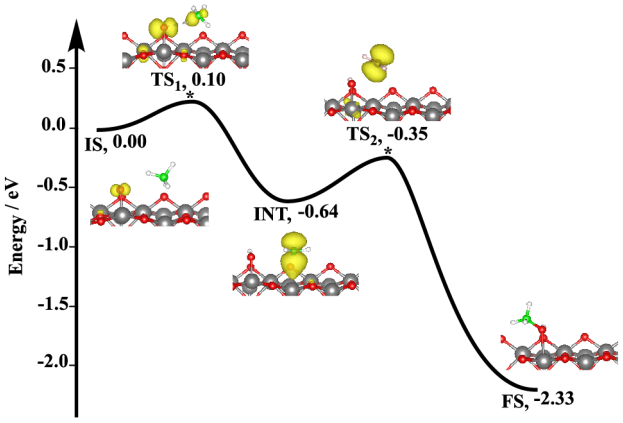

Figure 6. Energy profile and the spin density distributions of the process of CH_4 photooxidation on the oxidized R-TiO_2(110) surfaces. The Ti, O, C, and H atoms are represented as gray, red, green, and white spheres, respectively. And the yellow area represents the spin density of electron clouds.

radical-rebound process[19] (Final state, FS) with a moderate energy barrier of 0.29 eV (Transient State 2, TS_2). While, the desorption energy of $CH_3^\bullet$ radical is only 0.18 eV, and the ΔG for the desorption of $CH_3^\bullet$ radical (1 atm, 60 K) is 0.11 eV. Under our experimental conditions (5×10^{-11} Torr, 60 K), the ΔG for the desorption of $CH_3^\bullet$ radical decreases from 0.11 eV to −0.04 eV. As a result, $CH_3^\bullet$ radicals can either desorb from the surface or migrate over the surface, leading to the CH_3OH production. Compared to the intermediate state (INT), the formation of CH_3OH at the ground state in the FS is greatly exothermic by 1.69 eV due to the deexcitation process. In comparison to the thermal cases (Figure 5a,b), the much smaller energy barriers and stronger exothermic effect suggest that CH_4 photooxidation could occur efficiently with the assistance of the hole-trapped dangling O_{Ti}^- on oxidized R-TiO_2(110).

DISCUSSION

Generally, CH_4 activation on solid surfaces can occur via direct or precursor-mediated mechanisms.[4,6] Recently, the thermocatalytic activation C−H of CH_4 has been achieved on rutile IrO_2(110) (the same surface structure as R-TiO_2(110))

https://doi.org/10.1021/jacsau.3c00771
JACS Au 2024, 4, 1396−1404

following the precursor-mediated mechanism, where CH_4 molecularly adsorbs as a strongly bound σ-complex on $IrO_2(110)$, resulting in the C−H bond cleavage at 150 K.[6] Theoretical calculations proposed[39] that the empty d_z^2 orbital of the Ir atoms accepts the electron donated from the C−H σ-bond, accompanied by a filled d_{xy} orbital for the back-bonding to the C−H antibonding orbital, leading to the heterolytic proton-coupled electron transfer (PCET) process of CH_4.[5,8] However, although the Ti_{5c} sites of R-$TiO_2(110)$ are also coordinatively unsaturated electron-deficient sites, the location of d_z^2 bands is far away from the Fermi level, resulting in almost no interaction with CH_4.[40] Either on the stoichiometric or oxidized R-$TiO_2(110)$ surfaces, $CH_{4(Ti)}$ only weakly adsorbs on the surfaces with an E_{ads} of about 0.30 eV, which is much smaller than the energy barrier (>1.0 eV) of thermocatalytic C−H bond activation of CH_4 on both the stoichiometric and oxidized R-$TiO_2(110)$ surfaces. The desorption of CH_4 molecules will occur preferentially instead of C−H bond activation during the TPD process.[40,41]

For photocatalytic CH_4 activation, a similar precursor-mediated mechanism is also proposed when a localized electrostatic field formed by electron-rich sites exists on the surface of catalysts.[5] The electron-rich sites can polarize the C−H bond to produce the σ-bonded M-CH_3 species. Then, photogenerated holes transfer to the polarized C−H bond, resulting in a homolytic dissociation of CH_4 and coupling into C_2H_6.[42−45] However, the low desorption temperature of CH_4 on R-$TiO_2(110)$ indicates that no σ-bonded M-CH_3 species is formed. Alternatively, according to previous research on photocatalytic CH_4 and C_3H_8 activation on TiO_2,[7,8,32] CH_4 photooxidation on the oxidized $TiO_2(110)$ surface is more likely to follow the hole-trapped O_{Ti}^--mediated Eley−Rideal (E−R) reaction pathway,[4,46] in which CH_4 weakly adsorbs and facilely migrates on the oxidized surface. When movable CH_4 molecules efficiently collide with the hole-trapped O_{Ti}^- centers adsorbed on the surface, one H atom of CH_4 molecule is extracted by the electrophilic O_{Ti}^- center via a homolytic process, forming $CH_3^\bullet$ radicals and OH groups (Figure 6).[47] Then, a small part of $CH_3^\bullet$ radicals rebound to O_{Ti}, HO_{Ti}, or O_b on the surface, forming CH_3O_{Ti}, CH_3OH_{Ti}, and CH_3O_b species, respectively. The CH_3O_b species has no photoreactivity, while the other two can be converted into CH_2O under photocatalysis.[37]

If a large amount of $OH^\bullet$ or $OOH^\bullet$ exists near the TiO_2 surface or in the gas phase, CH_3OH and CH_3OOH can be easily formed via the reaction of the $CH_3^\bullet$ radical with these species.[3,7,17,19] Then, the composition (such as $OH^\bullet$ from H_2O or H_2O_2, $OOH^\bullet$ from O_2) and concentration of oxygen species in the gas phase will determine the final products from $CH_3^\bullet$ radicals, which change corresponding to different target products. In addition, by modifying the catalyst surface with transition metals (e.g., Au and Ag) to increase the interaction between $CH_3^\bullet$ radicals and catalyst surfaces,[2,19] photocatalytic oxidative coupling of CH_4 via a heterogeneous mechanism will occur more easily. Therefore, the interaction between $CH_3^\bullet$ radicals and catalyst surfaces and the oxygen species in the gas phase under ambient pressure jointly determine the heterogeneous catalytic mechanism and final products of photocatalytic CH_4 oxidation.

These results show that the surface-adsorbed O atom (O_{Ti} on R-$TiO_2(110)$) is not only regarded as a strong scavenger of excess electrons on the surface for promoting the photocatalytic reactivity but also directly induces the C−H bond activation. Furthermore, as shown in Figure S3, only $H_2{}^{18}O$ forms on the $^{18}O_{Ti}$ atoms precovered R-$TiO_2(110)$ under UV irradiation, further indicating that hole- trapped O_b^- is not involved in the C−H bond cleavage of CH_4. However, according to Wang's DFT results, hole-trapped O_b^- on R-$TiO_2(110)$ can readily abstract the H atom via a HAT process.[8] In addition, in the photocatalytic oxidative CH_4 conversion into CH_2O over the biphase TiO_2 catalyst under ambient conditions, Tang and coworkers[7] reported that the biphase TiO_2 catalyst can enhance electron−hole separation with a hole located at the rutile phase, and the photogenerated lattice O^- species on the rutile phase are consumed to activate the C−H bond of CH_4, forming O_v. Then, the O_v sites are rehealed by O_2 feed gas. As a result, photocatalytic oxidative CH_4 conversion over the biphase TiO_2 catalyst is achieved following the Mars−van−Krevelen (MvK) mechanism.[7] Moreover the biphase TiO_2 catalyst (90% anatase-TiO_2) was totally converted into pure rutile phase with the existence of (110) facet at >800 °C, the pure rutile phase also shows a good performance of CH_2O production under Xe lamp irradiation (a wavelength range of 300−1100 nm). In addition, the active lattice O^- species on the rutile surface has been identified by the low-temperature electron spin resonance (ESR) spectroscopy,[7] indicating that hole-trapped O_b^- shows high reactivity in photocatalytic oxidative CH_4 conversion on the rutile TiO_2 phase under ambient conditions. Similarly, the lattice oxygen-catalyzed CH_4 activation following the MvK mechanism has also been proposed in ZnO photocatalytic systems.[18,19]

Likewise, hole-trapped O_b^- can also induce dehydrogenation of toluene and ethylbenzene (EB) that contain active α-H atoms on reduced R-$TiO_2(110)$ with 355 nm irradiation under ultrahigh vacuum (UHV) conditions.[48,49] However, no observation of photocatalytic CH_4 dehydrogenation on reduced R-$TiO_2(110)$ indicates that the activity of hole-trapped lattice O_b^- is lower than that of hole-trapped O_{Ti}^- under 355 nm irradiation. The different activities of these two species on oxidized R-$TiO_2(110)$ may be due to two reasons. First, since the C−H bond activation is likely to occur via the E−R mechanism, the reaction can be regarded as the collision between CH_4 molecules and holes trapped in either O_{Ti}^- or O_b^-. The reaction will be competitive with hot-hole thermalization. The different rates of relaxation of the hole-trapped in O_{Ti}^- and in O_b^- will also affect the activity of these two species.

Besides, the adsorption structure of CH_4 may affect the collision. As shown in Figure 6, CH_4 molecules only physically adsorbs at the Ti_{5c} sites, the adsorption temperature of CH_4 on the O_b sites of R-$TiO_2(110)$ is still about 15 K lower than that on the Ti_{5c} sites.[24] Therefore, due to the corrugated structure of the R-$TiO_2(110)$ surface, the CH_4 molecule may migrate along the Ti_{5c} rows at low temperatures easily. Because CH_4 weakly adsorbs on the Ti_{5c} sites of R-$TiO_2(110)$, the height of the CH_4 molecule from the Ti_{5c} site plane is higher than that of the dangling hole trapped in O_{Ti}^- (Figure 6). Then, the collision between CH_4 and hole-trapped O_{Ti}^- will be a grazing incidence collision because of the large impact parameter, in which the CH_4 molecule will skim over the hole- trapped O_{Ti}^-. As a result, most of the $CH_3^\bullet$ radicals are ejected into a vacuum via the grazing collision manner. In addition, the CH_4 molecule is much higher than the O_b site. Then, the collision between the CH_4 molecule and hole-trapped O_{Ti}^- is more effective than that between the CH_4 molecule and hole-trapped O_b^-, which may also affect the activity of these two species.

https://doi.org/10.1021/jacsau.3c00771
JACS Au 2024, 4, 1396−1404

In addition, the difference in the results under UHV conditions and ambient conditions may be due to three possible reasons. First, under ambient conditions, the dissociative adsorption of O_2 at the O_v sites may also produce O_{Ti} on TiO_2. However, compared to the coverage of O_b on the surface, the concentration of the O_{Ti} produced via the dissociative adsorption of O_2 at the O_v sites is much lower. As a result, it is difficult for the ESR to distinguish hole-trapped O_{Ti}^- from the hole-trapped lattice O_b^- under irradiation. Besides, the reaction temperature is usually higher than room temperature under ambient conditions. At room temperature, the interaction of the CH_4 molecule with the catalysts will form a quick balance between desorption and adsorption. Namely, the collisions between the gas-phase CH_4 and the surface of the catalyst will occur many times per second. Thus, the translation normal to the surface of the CH_4 molecule in the gas phase will make the collision with hole-trapped O_b^- more effective, which is distinct from the case on R-TiO_2(110) at low surface temperatures. Further, previous works suggest that charge carrier thermalization may be accelerated at higher surface temperatures.[50] Therefore, the C−H bond activation may occur with relaxed hole trapped in O_{Ti}^- and O_b^- under ambient conditions. The activity of the relaxed hole-trapped O_{Ti}^- and O_b^- may not show a significant difference, resulting in the difficulty in distinguishing the hole-trapped O_{Ti}^- from the hole-trapped lattice O_b^- as well. Here, we not only illustrate that hole-trapped O_{Ti}^- is also an extremely important site for CH_4 photooxidation on R-TiO_2(110), but also observe the important $CH_3^\bullet$ radical intermediate, which is crucial for unraveling the mechanism of photocatalytic CH_4 conversion.

CONCLUSIONS

In summary, we have systematically investigated CH_4 photooxidation on R-TiO_2(110), which has been achieved at ∼60 K on the O_{Ti} atoms covered surface, and the $CH_3^\bullet$ radical intermediate in the reaction is detected directly. The initial C−H bond activation occurs via the E−R reaction pathway, in which the hole-trapped O_{Ti}^- centers rather than the hole-trapped O_b^- centers are the active species, resulting in the formation of a $CH_3^\bullet$ radical intermediate. The result not only provides a solid mechanistic insight into CH_4 activation via photocatalysis utilizing experimental and theoretical methods, but also offers new opportunities for the design of improved catalysts for oxidative CH_4 conversion via photocatalysis with high efficiency and selectivity.

METHODS

Experimental Section

All the TPD experiments were conducted with a home-built apparatus, and the details of the apparatus and experimental methods have been previously described.[32,51] Briefly, the well-ordered R-TiO_2(110) surfaces (10 mm × 10 mm × 1 mm, Princeton Scientific Corp.) were prepared by cycles of Ar^+ sputtering and UHV annealing at 900 K. The purities of the CH_4, O_2, and isotopic O_2^{18} gases were ≥99.99%. A 355 nm picosecond laser (BLAZER-UV, pulse duration: ∼15 ps; repetition rate: 2 MHz) was employed in the TPD and PSD experiments. The third harmonic output (343 nm) of a 1030 nm laser (Flare NX laser, Coherent; pulse duration: ∼1.5 ns; repetition rate: 200 Hz) was used for the TOF measurements. Both the power of the 355 and 343 nm were 5 mW, corresponding to a photon flux of about 2.0×10^{16} photons cm^{-2} s^{-1}.

Computational Section

The Vienna ab initio simulation package code[52,53] and plane augmented wave potential[54] were used for theoretical calculations. The wave function was expanded by the plane wave, with a kinetic cutoff of 400 eV and a density cutoff of 650 eV. The generalized gradient approximation with the spin-polarized Perdew−Burke−Ernzerhof functional[55] was used. Dispersion interactions are described by using the DFT-D3 van der Waals correction.[56] The transition states were searched using the climbing-image nudged elastic band approach (CI-NEB) method.[57]

A six-layer slab TiO_2 crystal was used as the surface model, and its (110) surface was exposed by cutting off a 4 × 2 surface unit cell. The periodically repeated slabs on the surface were decoupled by 15 Å vacuum gaps. A Monkhorst−Pack grid of (2 × 1 × 2) k-points was used for optimization.[58]

Three types of R-TiO_2(110) surfaces were used to study the C−H cleavage of CH_4: stoichiometric surface, oxidized surface, and photoexcited oxidized surface. The oxidized surface with O_{Ti} atom adsorption is simulated by adsorbing an O_{Ti} atom on the top of the slab and two OH groups on the O_b rows (OH_b) at the bottom of the slab to neutralize the unpaired electrons. Based on the previous result, the OH group can be used to introduce a hole into the surface by acting as an electron-withdrawing group,[59−61] To simulate the surface with a photoexcited hole, an O_{Ti} atom was added to the top of the slab with an OH_b at the bottom. In the final step of CH_4 activation by a photoexcited hole, the hole recombines with the electron trapped at the bottom of the slab to form CH_3OH in the ground state, adsorbed on the surface.

ASSOCIATED CONTENT

Supporting Information

The Supporting Information is available free of charge at https://pubs.acs.org/doi/10.1021/jacsau.3c00771.

Details of quantitative calculation; TPD spectra of CH_4 on R-TiO_2(110); the TPD spectra of formaldehyde (CH_2O); TPD spectra collected for CH_4 photooxidation on $^{18}O_{Ti}$ isotope covered R-TiO_2(110); discussion about the 650 K peak in the TPD spectrum at m/z = 15 in Figure 1; and TPD spectra of O_2 on R-TiO_2(110) (PDF)

AUTHOR INFORMATION

Corresponding Authors

Fangliang Li − *Shenzhen Key Laboratory of Energy Chemistry & Department of Chemistry, Southern University of Science and Technology, Shenzhen, Guangdong 518055, PR China;* orcid.org/0000-0002-0189-7564; Email: lifl@shanghaitech.edu.cn

Hongjun Fan − *State Key Laboratory of Molecular Reaction Dynamics, Dalian Institute of Chemical Physics, Chinese Academy of Sciences, Dalian, Liaoning 116023, PR China;* orcid.org/0000-0003-3406-6932; Email: Fanhj@dicp.ac.cn

Qing Guo − *Shenzhen Key Laboratory of Energy Chemistry & Department of Chemistry, Southern University of Science and Technology, Shenzhen, Guangdong 518055, PR China;* orcid.org/0000-0001-7029-3978; Email: guoq@sustech.edu.cn

Authors

Yuemiao Lai − *Shenzhen Key Laboratory of Energy Chemistry & Department of Chemistry, Southern University of Science and Technology, Shenzhen, Guangdong 518055, PR China;* orcid.org/0000-0002-4622-8225

https://doi.org/10.1021/jacsau.3c00771
JACS Au 2024, 4, 1396−1404

Ruimin Wang − *State Key Laboratory of Molecular Reaction Dynamics, Dalian Institute of Chemical Physics, Chinese Academy of Sciences, Dalian, Liaoning 116023, PR China; School of Pharmacy, North China University of Science and Technology, Tangshan, Hebei 063210, PR China*

Yi Zeng − *Shenzhen Key Laboratory of Energy Chemistry & Department of Chemistry, Southern University of Science and Technology, Shenzhen, Guangdong 518055, PR China*

Xiao Chen − *Shenzhen Key Laboratory of Energy Chemistry & Department of Chemistry, Southern University of Science and Technology, Shenzhen, Guangdong 518055, PR China; Institute of Advanced Science Facilities, Shenzhen, Guangdong 518107, PR China;* orcid.org/0000-0002-1356-7917

Tao Wang − *Shenzhen Key Laboratory of Energy Chemistry & Department of Chemistry, Southern University of Science and Technology, Shenzhen, Guangdong 518055, PR China;* orcid.org/0000-0002-6091-1020

Complete contact information is available at: https://pubs.acs.org/10.1021/jacsau.3c00771

Author Contributions

[#]Y.L. and R.W. contributed equally to this work.

Notes

The authors declare no competing financial interest.

ACKNOWLEDGMENTS

This work was supported by the National Key R&D Program of China (Grant No. 2018YFE0203002, 2022YFA1503102), the National Natural Science Foundation of China (Grant No. 22173041, 22103033, 22103031, 22173042, 21973037, 92061114, NSFC Center for Chemical Dynamics), the Strategic Priority Research Program of Chinese Academy of Sciences (Grant No. XDB17000000), the Shenzhen Science and Technology Innovation Committee (Grant No. 20220814164755002), the Guangdong Innovative & Entrepreneurial Research Team Program (Grant No. 2019ZT08L455, 2019JC01 × 091).

REFERENCES

(1) Xie, S.; Ma, W.; Wu, X.; Zhang, H.; Zhang, Q.; Wang, Y.; Wang, Y. Photocatalytic and electrocatalytic transformations of C1 molecules involving C−C coupling. *Energy Environ. Sci.* **2021**, *14*, 37−89.

(2) Song, S.; Song, H.; Li, L.; Wang, S.; Chu, W.; Peng, K.; Meng, X.; Wang, Q.; Deng, B.; Liu, Q. A Selective Au-ZnO/TiO_2 Hybrid Photocatalyst for Oxidative Coupling of Methane to Ethane with Dioxygen. *Nat. Catal.* **2021**, *4*, 1032−1042.

(3) Xie, J.; Jin, R.; Li, A.; Bi, Y.; Ruan, Q.; Deng, Y.; Zhang, Y.; Yao, S.; Sankar, G.; Ma, D. Highly Selective Oxidation of Methane to Methanol at Ambient Conditions by Titanium Dioxide-Supported Iron Species. *Nat. Catal.* **2018**, *1*, 889−896.

(4) Schwach, P.; Pan, X.; Bao, X. Direct Conversion of Methane to Value-Added Chemicals over Heterogeneous Catalysts: Challenges and Prospects. *Chem. Rev.* **2017**, *117*, 8497−8520.

(5) Li, Q.; Ouyang, Y.; Li, H.; Wang, L.; Zeng, J. Photocatalytic Conversion of Methane: Recent Advancements and Prospects. *Angew. Chem., Int. Ed.* **2022**, *134*, No. e202108069.

(6) Liang, Z.; Li, T.; Kim, M.; Asthagiri, A.; Weaver, J. F. Low-Temperature Activation of Methane on the IrO_2 (110) Surface. *Science* **2017**, *356*, 299−303.

(7) Jiang, Y.; Zhao, W.; Li, S.; Wang, S.; Fan, Y.; Wang, F.; Qiu, X.; Zhu, Y.; Zhang, Y.; Long, C.; Tang, Z. Elevating Photooxidation of Methane to Formaldehyde via TiO_2 Crystal Phase Engineering. *J. Am. Chem. Soc.* **2022**, *144*, 15977−15987.

(8) Zhou, M.; Wang, H. Optimally Selecting Photo- and Electrocatalysis to Facilitate CH 4 Activation on TiO 2 (110) Surface: Localized Photoexcitation versus Global Electric-Field Polarization. *JACS Au* **2022**, *2*, 188−196.

(9) Meng, X.; Cui, X.; Rajan, N. P.; Yu, L.; Deng, D.; Bao, X. Direct Methane Conversion under Mild Condition by Thermo-, Electro-, or Photocatalysis. *Chem* **2019**, *5*, 2296−2325.

(10) Jin, Z.; Wang, L.; Zuidema, E.; Mondal, K.; Zhang, M.; Zhang, J.; Wang, C.; Meng, X.; Yang, H.; Mesters, C. Hydrophobic Zeolite Modification for in Situ Peroxide Formation in Methane Oxidation to Methanol. *Science* **2020**, *367*, 193−197.

(11) Wang, Y.; Hu, P.; Yang, J.; Zhu, Y.-A.; Chen, D. C−H Bond Activation in Light Alkanes: A Theoretical Perspective. *Chem. Soc. Rev.* **2021**, *50*, 4299−4358.

(12) Chen, X.; Li, Y.; Pan, X.; Cortie, D.; Huang, X.; Yi, Z. Photocatalytic Oxidation of Methane over Silver Decorated Zinc Oxide Nanocatalysts. *Nat. Commun.* **2016**, *7*, 12273.

(13) Murcia-Lopez, S.; Villa, K.; Andreu, T.; Morante, J. R. Partial Oxidation of Methane to Methanol Using Bismuth-Based Photocatalysts. *ACS Catal.* **2014**, *4*, 3013−3019.

(14) Murcia-Lopez, S.; Bacariza, M. C.; Villa, K.; Lopes, J. M.; Henriques, C.; Morante, J. R.; Andreu, T. Controlled Photocatalytic Oxidation of Methane to Methanol through Surface Modification of Beta Zeolites. *ACS Catal.* **2017**, *7*, 2878−2885.

(15) Villa, K.; Murcia-López, S.; Andreu, T.; Morante, J. R. Mesoporous WO_3 Photocatalyst for the Partial Oxidation of Methane to Methanol Using Electron Scavengers. *Appl. Catal., B* **2015**, *163*, 150−155.

(16) Jiang, Y.; Li, S.; Wang, S.; Zhang, Y.; Long, C.; Xie, J.; Fan, X.; Zhao, W.; Xu, P.; Fan, Y. Enabling Specific Photocatalytic Methane Oxidation by Controlling Free Radical Type. *J. Am. Chem. Soc.* **2023**, *145*, 2698−2707.

(17) Song, H.; Meng, X.; Wang, S.; Zhou, W.; Wang, X.; Kako, T.; Ye, J. Direct and Selective Photocatalytic Oxidation of CH_4 to Oxygenates with O_2 on Cocatalysts/ZnO at Room Temperature in Water. *J. Am. Chem. Soc.* **2019**, *141*, 20507−20515.

(18) Wang, P.; Shi, R.; Zhao, Y.; Li, Z.; Zhao, J.; Zhao, J.; Waterhouse, G. I.; Wu, L.-Z.; Zhang, T. Selective Photocatalytic Oxidative Coupling of Methane via Regulating Methyl Intermediates over Metal/ZnO Nanoparticles. *Angew. Chem., Int. Ed.* **2023**, *62*, No. e202304301.

(19) Liu, C.; Qian, B.; Xiao, T.; Lv, C.; Luo, J.; Bao, J.; Pan, Y. Illustrating the Fate of Methyl Radical in Photocatalytic Methane Oxidation over Ag−ZnO by in situ Synchrotron Radiation Photoionization Mass Spectrometry. *Angew. Chem., Int. Ed.* **2023**, *62*, No. e202304352.

(20) Schröder, D.; Roithová, J. Low-Temperature Activation of Methane: It Also Works Without a Transition Metal. *Angew. Chem., Int. Ed.* **2006**, *45*, 5705−5708.

(21) Ito, T.; Tashiro, T.; Watanabe, T.; Kawasaki, M.; Toi, K.; Kobayashi, H. Adsorption of Methane on Magnesium Oxide Surfaces under Ultraviolet Irradiation. *J. Chem. Soc., Faraday Trans.* **1990**, *86*, 4071−4075.

(22) Lira, E.; Hansen, J. Ø.; Huo, P.; Bechstein, R.; Galliker, P.; Lægsgaard, E.; Hammer, B.; Wendt, S.; Besenbacher, F. Dissociative and Molecular Oxygen Chemisorption Channels on Reduced Rutile TiO_2 (110): An STM and TPD Study. *Surf. Sci.* **2010**, *604*, 1945−1960.

(23) Sokolović, I.; Reticcioli, M.; Čalkovský, M.; Wagner, M.; Schmid, M.; Franchini, C.; Diebold, U.; Setvín, M. Resolving the Adsorption of Molecular O_2 on the Rutile TiO_2(110) Surface by Noncontact Atomic Force Microscopy. *Proc. Natl. Acad. Sci. U. S. A.* **2020**, *117*, 14827−14837.

(24) Chen, L.; Smith, R. S.; Kay, B. D.; Dohnálek, Z. Adsorption of Small Hydrocarbons on Rutile TiO_2 (110). *Surf. Sci.* **2016**, *650*, 83−92.

(25) Henderson, M. A.; Epling, W. S.; Peden, C. H.; Perkins, C. L. Insights into Photoexcited Electron Scavenging Processes on TiO_2 Obtained from Studies of the Reaction of O_2 with OH Groups

Adsorbed at Electronic Defects on TiO_2 (110). *J. Phys. Chem. B* **2003**, *107*, 534−545.
(26) Yu, X.; Zhang, Z.; Yang, C.; Bebensee, F.; Heissler, S.; Nefedov, A.; Tang, M.; Ge, Q.; Chen, L.; Kay, B. D.; et al. Interaction of Formaldehyde with the Rutile TiO_2 (110) Surface: A Combined Experimental and Theoretical Study. *J. Phys. Chem. C* **2016**, *120*, 12626−12636.
(27) Lu, G.; Linsebigler, A.; Yates, J. T., Jr Ti^{3+} Defect Sites on TiO_2 (110): Production and Chemical Detection of Active Sites. *J. Phys. Chem.* **1994**, *98*, 11733−11738.
(28) Thompson, T. L.; Yates, J. T. Monitoring Hole Trapping in Photoexcited TiO_2 (110) Using a Surface Photoreaction. *J. Phys. Chem. B* **2005**, *109*, 18230−18236.
(29) Driscoll, D. J.; Martir, W.; Wang, J. X.; Lunsford, J. H. Formation of Gas-Phase Methyl Radicals over Magnesium Oxide. *J. Am. Chem. Soc.* **1985**, *107*, 58−63.
(30) Lunsford, J. H. The Role of Surface-Generated Gas-Phase Radicals in Catalysis. *Langmuir* **1989**, *5*, 12−16.
(31) Luo, L.; Tang, X.; Wang, W.; Wang, Y.; Sun, S.; Qi, F.; Huang, W. Methyl Radicals in Oxidative Coupling of Methane Directly Confirmed by Synchrotron VUV Photoionization Mass Spectroscopy. *Sci. Rep.* **2013**, *3*, 1625.
(32) Li, F.; Wang, B.; Chen, X.; Lai, Y.; Wang, T.; Fan, H.; Yang, X.; Guo, Q. Photocatalytic Oxidative Dehydrogenation of Propane for Selective Propene Production with TiO_2. *JACS Au* **2022**, *2*, 2607−2616.
(33) Roithova, J.; Schroder, D. Selective Activation of Alkanes by Gas-Phase Metal Ions. *Chem. Rev.* **2010**, *110*, 1170−1211.
(34) Nandy, A.; Kulik, H. J. Why Conventional Design Rules for C−H Activation Fail for Open-Shell Transition-Metal Catalysts. *ACS Catal.* **2020**, *10*, 15033−15047.
(35) Vitillo, J. G.; Bhan, A.; Cramer, C. J.; Lu, C. C.; Gagliardi, L. Quantum Chemical Characterization of Structural Single Fe(II) Sites in MIL-Type Metal−Organic Frameworks for the Oxidation of Methane to Methanol and Ethane to Ethanol. *ACS Catal.* **2019**, *9*, 2870−2879.
(36) Mahyuddin, M. H.; Shiota, Y.; Staykov, A.; Yoshizawa, K. Theoretical Investigation of Methane Hydroxylation over Isoelectronic $[FeO]^{2+}$- and $[MnO]^{+}$-Exchanged Zeolites Activated by N_2O. *Inorg. Chem.* **2017**, *56*, 10370−10380.
(37) Guo, Q.; Xu, C.; Ren, Z.; Yang, W.; Ma, Z.; Dai, D.; Fan, H.; Minton, T. K.; Yang, X. Stepwise Photocatalytic Dissociation of Methanol and Water on TiO_2 (110). *J. Am. Chem. Soc.* **2012**, *134*, 13366−13373.
(38) Adachi, Y.; Sugawara, Y.; Li, Y. J. Remotely Controlling the Charge State of Oxygen Adatoms on a Rutile TiO_2 (110) Surface Using Atomic Force Microscopy. *J. Phys. Chem. C* **2020**, *124*, 12010−12015.
(39) Wang, C.-C.; Siao, S. S.; Jiang, J.-C. C-H Bond Activation of Methane via σ-d Interaction on the IrO_2 (110) Surface: Density Functional Theory Study. *J. Phys. Chem. C* **2012**, *116*, 6367−6370.
(40) Fung, V.; Tao, F. F.; Jiang, D. Low-Temperature Activation of Methane on Doped Single Atoms: Descriptor and Prediction. *Phys. Chem. Chem. Phys.* **2018**, *20*, 22909−22914.
(41) Fung, V.; Hu, G.; Tao, F.; Jiang, D. Methane Chemisorption on Oxide-Supported Pt Single Atom. *ChemPhyschem* **2019**, *20*, 2217−2220.
(42) Meng, L.; Chen, Z.; Ma, Z.; He, S.; Hou, Y.; Li, H. H.; Yuan, R.; Huang, X. H.; Wang, X.; Wang, X.; et al. Gold Plasmon-Induced Photocatalytic Dehydrogenative Coupling of Methane to Ethane on Polar Oxide Surfaces. *Energy Environ. Sci.* **2018**, *11*, 294−298.
(43) Li, L.; Cai, Y. Y.; Li, G. D.; Mu, X. Y.; Wang, K. X.; Chen, J. S. Synergistic Effect on the Photoactivation of the Methane C-H Bond over Ga^{3+}-Modified ETS-10. *Angew. Chem., Int. Ed. Engl.* **2012**, *51*, 4702−4706.
(44) Li, L.; Fan, S.; Mu, X.; Mi, Z.; Li, C. J. Photoinduced Conversion of Methane into Benzene over GaN Nanowires. *J. Am. Chem. Soc.* **2014**, *136*, 7793−7796.
(45) Tang, C.; Du, S.; Huang, H.; Tan, S.; Zhao, J.; Zhang, H.; Ni, W.; Yue, X.; Ding, Z.; Zhang, Z. Au−Pd Tandem Photocatalysis for Nonoxidative Coupling of Methane toward Ethylene. *ACS Catal.* **2023**, *13*, 6683−6689.
(46) Kraus, P.; Lindstedt, R. P. It's a Gas: Oxidative Dehydrogenation of Propane over Boron Nitride Catalysts. *J. Phys. Chem. C* **2021**, *125*, 5623−5634.
(47) Zhang, J.; Shen, J.; Li, D.; Long, J.; Gao, X.; Feng, W.; Zhang, S.; Zhang, Z.; Wang, X.; Yang, W. Efficiently Light-Driven Nonoxidative Coupling of Methane on $Ag/NaTaO_3$: A Case for Molecular-Level Understanding of the Coupling Mechanism. *ACS Catal.* **2023**, *13*, 2094−2105.
(48) Li, F.; Wang, B.; Chen, X.; Zeng, W.; Sun, R.; Liu, X.; Ren, Z.; Yang, X.; Fang, H.; Guo, Q. Photocatalytic C-H bond Activation of Toluene on Rutile TiO_2(110). *J. Phys. Chem. C* **2022**, *126*, 11963−11970.
(49) Li, F.; Chen, X.; Lai, Y.; Wang, T.; Yang, X.; Guo, Q. Low-Temperature C-H Bond Activation via Photocatalysis: Highly Efficient Ethylbenzene Dehydrogenation into Styrene on Rutile TiO_2(110). *J. Phys. Chem. Lett.* **2022**, *13*, 9186−9194.
(50) Henderson, M. A. A Surface Science Perspective on TiO_2 Photocatalysis. *Surf. Sci. Rep.* **2011**, *66*, 185−297.
(51) Ren, Z.; Guo, Q.; Xu, C.; Yang, W.; Xiao, C.; Dai, D.; Yang, X. Surface Photocatalysis-TPD Spectrometer for Photochemical Kinetics. *Chin. J. Chem. Phys.* **2012**, *25*, 507.
(52) Kresse, G.; Furthmüller, J. Efficiency of Ab-Initio Total Energy Calculations for Metals and Semiconductors Using a Plane-Wave Basis Set. *Comput. Mater. Sci.* **1996**, *6*, 15−50.
(53) Kresse, G.; Furthmüller, J. Efficient Iterative Schemes for Ab Initio Total-Energy Calculations Using a Plane-Wave Basis Set. *Phys. Rev. B* **1996**, *54*, 11169.
(54) Blöchl, P. E. Projector Augmented-Wave Method. *Phys. Rev. B* **1994**, *50*, 17953.
(55) Perdew, J. P.; Burke, K.; Ernzerhof, M. Generalized Gradient Approximation Made Simple. *Phys. Rev. Lett.* **1996**, *77*, 3865.
(56) Grimme, S.; Ehrlich, S.; Goerigk, L. Effect of the Damping Function in Dispersion Corrected Density Functional Theory. *J. Comput. Chem.* **2011**, *32*, 1456−1465.
(57) Henkelman, G.; Jonsson, H. Improved Tangent Estimate in the Nudged Elastic Band Method for Finding Minimum Energy Paths and Saddle Points. *J. Chem. Phys.* **2000**, *113*, 9978−9985.
(58) Monkhorst, H. J.; Pack, J. D. Special Points for Brillouin-Zone Integrations. *Phys. Rev. B* **1976**, *13*, 5188.
(59) Ji, Y.; Wang, B.; Luo, Y. GGA+U Study on the Mechanism of Photodecomposition of Water Adsorbed on Rutile TiO_2(110) Surface: Free vs Trapped Hole. *J. Phys. Chem. C* **2014**, *118*, 1027−1034.
(60) Wang, D.; Wang, H.; Hu, P. Identifying the Distinct Features of Geometric Structures for Hole Trapping to Generate Radicals on Rutile TiO_2(110) in Photooxidation Using Density Functional Theory Calculations with Hybrid Functional. *Phys. Chem. Chem. Phys.* **2015**, *17*, 1549−1555.
(61) Zhang, J.; Peng, C.; Wang, H.; Hu, P. Identifying the Role of Photogenerated Holes in Photocatalytic Methanol Dissociation on Rutile TiO_2(110). *ACS Catal.* **2017**, *7*, 2374−2380.

https://doi.org/10.1021/jacsau.3c00771
JACS Au 2024, 4, 1396−1404